Surfactant-Modified CO_2−Water Interface: A Molecular View

Sandro R. P. da Rocha,[†,§] Keith P. Johnston,[‡,§] and Peter J. Rossky*[,†,‡,§]

Institute for Theoretical Chemistry, Department of Chemistry and Biochemistry, Department of Chemical Engineering, and NSF-STC−Environmentally Responsible Solvents and Processes, The University of Texas at Austin, Austin, Texas 78712-1167

Received: June 25, 2002; In Final Form: September 21, 2002

An important goal is the design of economically viable amphiphiles capable of forming and stabilizing water domains in bulk CO_2. To enhance the understanding of this class of systems, we present in this work the results from atomistic molecular dynamics computer simulations of a perfluoropolyether ammonium carboxylate surfactant monolayer at the high-pressure CO_2|water interface. The system is modeled including all internal degrees of freedom for the surfactant anion, and considering all atoms explicitly. At 318 K and 23 MPa, and 84 Å^2/molecule surface coverage, the calculated decrement in interfacial tension due to the presence of the monolayer agrees with the experimental value previously obtained in our laboratories. We show that the surfactant monolayer retains most of the structural features commonly observed in conventional hydrocarbon amphiphiles at the oil|water interface. However, CO_2 penetrates the surfactant monolayer to a larger extent than conventional hydrocarbon solvents. Correspondingly, CO_2 is also capable of solvating the fluorinated tail-group throughout. The result is a thick, fairly structured monolayer, comparable to analogous hydrocarbon surfactants at the oil|water interface, a surprising observation given the much lower surfactant surface coverage. On the aqueous side, in contrast, the carboxylic carbon is well solvated, but very little contact between water and the tail-group is observed past the CF2 adjacent to the head-group. It is also observed that most of the ammonium counterions are associated with the head-groups.

I. Introduction

Surfaces and interfaces modified by amphiphilic molecules are of great fundamental and technological relevance in areas including drug delivery, biosensing, particle formation, lubrication, and in the production of biomimetic materials.[1−4] To a large extent, the physicochemical properties of interfaces are dictated by the interfacial structure.[5] The characterization of this nanometer-size region is, therefore, of vital importance. While a wealth of experimental techniques are available for the determination of the microscopic properties of modified solid−air/vacuum interfaces,[6] fewer are suitable for fluid−air interfaces.[4] The scenario is further complicated for buried systems, such as surfactant monolayers at oil−water (O|W) interfaces.[5,7]

A fundamental understanding of the behavior of amphiphiles at O|W interfaces is required for the development of emulsion and microemulsion science. For example, the preferred interfacial curvature and monolayer bending elasticity of fluid−fluid interfaces are thought to be dictated by the degree of penetration of oil in the surfactant tail region.[8] Experimental techniques such as X-ray[9] and neutron reflectivity[10,11] as well as sum frequency vibrational spectroscopy[12] have all given insight into the structural organization of buried monolayers located at the interface of immiscible fluids, providing molecular level information such as volume fraction profiles,[8] degree of order and thickness of the monolayer,[9] counterion distribution,[13] and solvent orientation.[14] The effect of surfactant head-group charge,[8,15] tail characteristics,[16,17] oil−surfactant tail interaction,[9] and of surfactant mixtures on monolayer characteristics have also been investigated.[10]

Even though, in principle, these novel techniques can be applied to any buried interfacial system, intrinsic limitations exist due to the fact that all liquids scatter and/or absorb neutrons and X-rays strongly,[7] and also absorb significantly in the infrared spectral region of interest.[5] This has severely restricted their practical applicability. On the other hand, with the advent of faster computers and novel algorithms[18] as well as reliable transferable potential models,[19,20] molecular dynamics (MD) computer simulation has become a powerful tool for the study of the microscopic structural and dynamical properties of fluid interfaces, serving as both a source of complementary information and a guide to experiments. While extensive literature is available for MD studies of surfactants at the air−water (A|W) interface,[21−27] only a few investigations have been reported for monolayers at O|W interfaces. Berkowitz and co-workers have investigated the structure and dynamics of a typical anionic surfactant, sodium dodecyl sulfate (SDS), at low and high surface coverage, at both the A|W and CCl_4|W interface.[28−30] The effect of head-group charge was also explored, by reversing the charge of the SDS anion and counterion.[28] The structure of the modified dodecane|W interface with a nonionic monododecyl pentaethylene glycol surfactant was the subject of a recent study by Kuhn and Rehage.[31]

In this work, we investigate the structure of a perfluoropolyether ammonium carboxylate surfactant monolayer at the CO_2|W (C|W) interface at high pressure using atomistic MD simulations. Dispersions of water and CO_2 in the form of microemulsions or emulsions are environmentally acceptable systems that offer new possibilities in areas including reactions,[32] protein extraction and separation,[33,34] bioconversion,[35,36] and materials

* Corresponding author.
† Institute for Theoretical Chemistry, Department of Chemistry and Biochemistry.
‡ Department of Chemical Engineering.
§ NSF-STC−Environmentally Responsible Solvents and Processes.

10.1021/jp021485b CCC: $22.00
Published on Web 12/02/2002

TABLE 1: Intermolecular Potential Parameters and Geometry for SPC/E Water,[a] EPM2 CO_2,[b] and OPLS NH_4^+ Cation[c]

	SPC/E water		EPM2 CO_2		OPLS NH_4^+
α^1 (°)	109.5	r_{C-O} (Å)	1.149	α (°)	tetrahedral
r_{O-H} (Å)	1.000	σ_C (Å)	2.757	r_{N-H} (Å)	1.010
σ_O (Å)	3.166	ϵ_C (kJ/mol)	0.234	σ_N (Å)	3.250
ϵ_O (kJ/mol)	0.650	σ_O (Å)	3.033	ϵ_N (kJ/mol)	0.712
σ_H (Å)	0.000	ϵ_O (kJ/mol)	0.669	σ_H (Å)	0.000
ϵ_H (kJ/mol)	0.000	σ_{CO} (Å)	2.892	ϵ_H (kJ/mol)	0.000
q_O (|e|)	−0.8476	ϵ_{CO} (kJ/mol)	0.396	q_N (|e|)	−0.400
q_H (|e|)	+0.4238	q_C (|e|)	+0.6512	q_H (|e|)	+0.350
		q_O (|e|)	−0.3256		

[a] Ref 50. [b] Ref 52. [c] Ref 58. [d] $-\angle_{OHO}$.

formation.[37,38] Because CO_2 has low polarizability density,[39] low dielectric constant,[40] and intrinsic transport properties such as low viscosity and high solute diffusivity,[41] the formation and stabilization of water domains in CO_2 is a more challenging problem compared to that of conventional organic solvents.[42,43] This work is the first step toward the development of a molecular level understanding of the behavior of amphiphiles capable of imparting stability to this novel interface.

Previous atomistic MD simulations of the C|W interface include our work, which focused on the details of the structure of the bare interface,[44] and that of Wipff and co-workers.[45−47] The latter focused on the behavior of ionic species in the interfacial region, in the context of liquid−liquid extraction. Cummings and co-workers have reported studies of a surfactant|C|W micelle.[48] In their work, they report the spontaneous formation and structure of a partially fluorinated dichain sulfosuccinate assembly, using a united-atom model description of the tail.

The organization of the present article is as follows. In Section II, we present the Computational Model and Simulation Methods. We use a fully atomistic approach for solvents and the amphiphile. All surfactant internal degrees of freedom, i.e., bond length, angle, and torsion, are treated explicitly. The simulation is performed at 318.15 K and 23 MPa, conditions typically used in the laboratory.[49] In Section III, Results and Discussion, thermodynamic and microstructural properties of the interfacial region, including interfacial tension, number density profiles, average monolayer tilt angle, fraction of gauche defects, order parameter, and thickness, are reported. We also characterize the monolayer with regard to the solvent−solute interaction. Wherever possible, the results are compared with those obtained experimentally for the C|W interface and to those of surfactant-modified conventional O|W interfaces. The C|W system has an unusually low surface coverage of amphiphiles at the C|W interface, compared to O|W systems, which we have attributed to the lower free energy density difference of this interface compared to O|W systems.[49] We will show that this low coverage has a large impact on the structural and thus on the physicochemical properties of the interfacial region. Conclusions and future directions are given in Section IV.

II. Computational Model and Simulation Methodology

2.1. Molecular Models and Potentials. Four molecular species are present in the simulation. Water is represented by the SPC/E model of Berendsen and co-workers,[50] with intermolecular potential parameters and geometry as given in Table 1. When accounting for the long-range electrostatic interaction with the Ewald summation technique, the SPC/E model has been shown to quantitatively describe the effect of temperature on the surface tension of pure water (water|vacuum interface).[51]

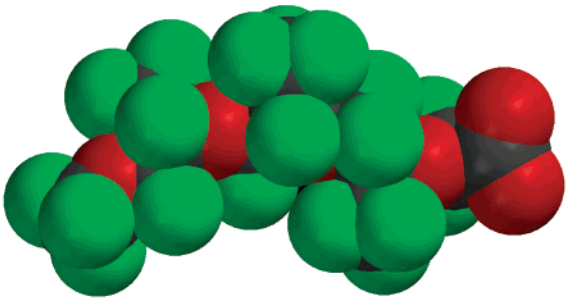

Figure 1. Space-filling model of the optimized gas-phase conformation for the surfactant anion under the AM1 electronic structure approximation. Calculations were performed using Spartan.[54]

Very accurate values for the interfacial tension (γ) of CCl_4|W were also obtained using the Ewald technique.[30] The EPM2 model, also with rigid geometry, is used for CO_2, with parameters as shown in Table 1.[52] This model consists of 3 Lennard-Jones (LJ) sites and three point charges located in the center of the LJ sites. The parameters for this potential model were fitted to reproduce the CO_2 vapor−liquid coexistence curve.[52] Our previous study has shown that γ for the binary CO_2−water (C|W) interface ($\gamma_{C|W}$)[44] calculated from MD simulations using the SPC/E and EPM2 models, with conventional combining rules, is in fair agreement with our experimental results obtained from high-pressure pendant drop tensiometry.[53]

An all-atom approach is used for the perfluoropolyether ammonium carboxylate surfactant, $CF_3(OCF_2CF(CF_3))_3OCF_2COO^-NH_4^+$, $M_w = 695.13$ (PFPE−$COO^-NH_4^+$). In Figure 1, we show a space-filling model of the anion in a structure optimized in the gas phase under the AM1 electronic structure approximation using Spartan.[54] The LJ, intramolecular parameters, and partial charges for the PFPE−COO^- are taken from the CVFF force field,[55−57] and are given in Tables 2 and 3. This force field has been employed previously to model the tribological behavior of branched and linear PFPEs and perfluoroalkanes.[56,57] The ammonium counterion (NH_4^+) is represented by a rigid model with 5-point charges and an LJ site on the central N atom.[58] The force field for the NH_4^+ ion was validated by comparing quantum mechanical calculations to Monte Carlo computer simulations of the cation in aqueous solutions.[58] The parameters for NH_4^+ are also shown in Table 1.

The total energy of the simulated system is the sum of the intra- and intermolecular interactions. The intramolecular interactions for the PFPE−COO^- anion are represented as a sum of four terms:

$$E_{intra} = \sum E_{stretch} + \sum E_{bend} + \sum E_{torsion} + \sum E_{out-of-plane} \quad (1)$$

The bond stretching term is given by

$$E_{stretch} = \sum_i H_i^b (b - b_0)^2 \quad (2)$$

where H_i^b is the ith bond stretching force constant, b_0 is the equilibrium bond length, and b is the actual bond length. The bond angle bending term is given by

$$E_{bend} = \sum_i H_i^\theta (\theta - \theta_0)^2 \quad (3)$$

where H_i^θ is the ith bond angle bending force constant, θ_0 is the equilibrium bond angle, and θ is the actual bond angle. The

TABLE 2: Lennard-Jones and Intramolecular Potential Parameters for the PFPE−COO⁻ Anion[55−57]

atom type	
C	alkyl carbon
C⁻	carbon in charged carboxylate
O	ether oxygen
O⁻	oxygen in charged carboxylate
F	alkyl fluorine

atom type	σ_{ii} (Å)	ϵ_{ii} (kJ/mol)	mass (amu)
C	3.474	0.670	12.0
C⁻	3.617	0.620	12.0
O	2.860	0.955	16.0
O⁻	2.860	0.955	16.0
F	3.081	0.288	19.0

bond length	H_i^b (kJ mol^{-1} Å^{-2})	b_0 (Å^2)
C−C	1351.1465	1.5260
C−F	2076.6528	1.3630
C−O	1143.8338	1.4250
C⁻−C	1185.2513	1.5200
C⁻−O⁻	2260.8720	1.2500

bond angle	H_i^θ (kJ mol^{-1} rad^{-2})	θ_0 (°)
C−C−C	195.1049	110.50
C−O−C	251.2080	109.50
F−C−O	397.7460	107.80
F−C−C	414.4932	107.80
F−C−F	397.7460	107.80
C−C−O	293.0760	109.50
F−C−C⁻	414.4932	107.80
C−C⁻-O⁻	284.7024	120.00
O−C−C⁻	293.0760	109.50
O⁻−C⁻−O⁻	607.0860	123.00

torsion	H_i^ϕ (kJ mol^{-1} rad^{-1})	n	ϕ_o (°)
−C−C−	5.9557	3	0.00
−C−O−	1.6328	3	0.00
−C−C⁻−	0.0000	0	0.00

out-of-plane	H_i^χ (kJ mol^{-1} rad^{-1})	n	χ_o (°)
C−C⁻−O⁻−O⁻	48.5669	2	180.00

TABLE 3: List of Partial Charges for the PFPE−COO⁻ Anion[a,b]

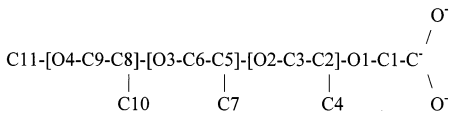

Atom Type	charge (|e|)	Atom Type	charge (|e|)
C3,C6,C9	0.700	C11	0.975
C2,C5,C8	0.425	O1,O2,O3,O4	- 0.300
C4,C7,C10	0.825	O-	- 0.570
C1	0.700	F	- 0.275
C-	0.140		

[a] Atoms within different repeat units [$OCF_2CF_2(CF_3)$] are equivalent, but are labeled individually for structural analysis. The explicit fluorine-carbon bonds are not shown for clarity. [b] Ref 55.

torsional and out-of-plane contribution to the intramolecular potential are represented by

$$E_{\text{torsion}} = \sum_i H_i^\phi (1 + \cos(n\phi - \phi_0)) \quad (4)$$

$$E_{\text{out-of-plane}} = \sum_i H_i^\chi (1 + \cos(n\chi - \chi_0)) \quad (5)$$

where H_i^ϕ and H_i^χ are the ith torsional and out-of-plane force constants, respectively, n is the periodicity, and ϕ and χ are the torsional angle and out-of-plane bending angle, respectively.

The intermolecular interactions between nonbonded pairs are given by a sum of a dispersion and an electrostatic term:

$$E_{\text{inter}} = \sum E_{\text{vdW}} + \sum E_{\text{electrostatic}} \quad (6)$$

The van der Waals interactions are accounted for with the 12-6 LJ potential model. The resulting equation for the E_{inter} is given by eq 7:

$$E_{\text{inter}} = \sum_i \sum_{j>i} \left\{ 4\epsilon_{ij} \left[\left(\frac{\sigma_{ij}}{r_{ij}}\right)^{12} - \left(\frac{\sigma_{ij}}{r_{ij}}\right)^{6} \right] + \frac{1}{4\pi\epsilon_0} \frac{q_i q_j}{r_{ij}} \right\} \quad (7)$$

where q_i and q_j are the charges centered on the individual atoms of different molecules, and r_{ij} is the distance between the sites i and j. σ_{ij} and ϵ_{ij} are the size and energy parameters for the LJ potential. The LJ parameters for the interactions between dissimilar atoms are calculated using the standard Lorentz−Berthelot combining and mixing rules given by eq 8,

$$\epsilon_{ij} = (\epsilon_{ii}\epsilon_{jj})^{1/2} \text{ and } \sigma_{ij} = 1/2(\sigma_{ii} + \sigma_{jj}) \quad (8)$$

except for that specified for C_cO_c (see Table 1).

2.2. Simulation Details. The system consists of 793 SPC/E water and 324 EPM2 CO_2 molecules, eight PFPE−COO^- anions, and eight NH_4^+ counterions. The initial configuration for the solvent molecules was obtained from the final coordinates of a 2 ns simulation of the binary SPC/E-EPM2 system at 318 K and 20 MPa,[44] the same target thermodynamic conditions as in this work. Both SPC/E and EPM2 molecules were translated in the direction perpendicular to the interface, i.e., z direction, creating an empty space where the surfactant molecules and counterions were positioned. Molecules with a z coordinated lower than the center of mass of the box ($z < 0$) were translated $-z$ Å, and the ones with $z > 0$, $+z$ Å, and the monolayer created in between.

The initial cross sectional area of the box ($L_x \times L_y$) was set to 30 × 30 Å, giving an initial area per surfactant head-group (A) of 112.5 Å^2. Such large areas at the critical microemulsion concentration ($c\mu c$) are typical for amphiphiles at the C|W interface.[53,59] All eight surfactant anions had the same initial conformation shown in Figure 1, and were arranged at one interface with the PFPE tail pointing into the bulk EPM2 CO_2 phase and the head-group pointing to the SPC/E water bulk side. The counterions were placed between the anions and the SPC/E bulk phase. Figure 2 is a snapshot of an equilibrium configuration of the system. For better visualization, only a region close to the interface is shown.

All simulations were carried out using the parallel version of DL_POLY 2.12,[60] on a PC cluster. Periodic boundary conditions were applied in all directions, in a way that two interfaces were present in the system: one with the surfactant monolayer, and a second consisting of a neat C|W interface. One of the other many possibilities would have been to treat two surfactant monolayers. In that case, however, one might expect possible interfacial correlations to demand a considerably larger size system. The present system allows us to evaluate the effect of interfacial correlations, if any, by comparing our second interface (C|W devoid of surfactant), with our previous study of the binary C|W interface.[44] The ease with which the interfacial tension for the modified interface ($\gamma_{C|W|S}$) can be calculated within the present setup was another reason for the

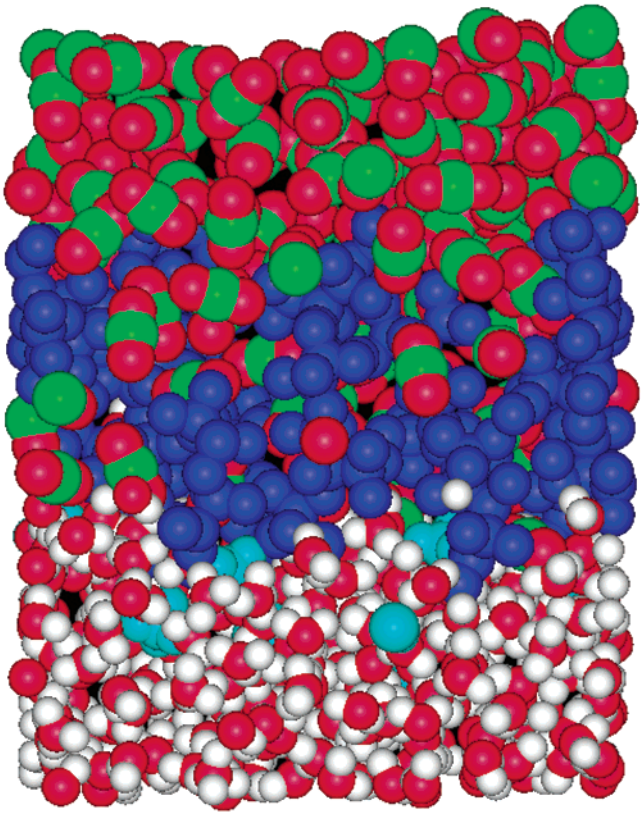

Figure 2. Snapshot of an equilibrium configuration of the interfacial region of the PFPE−$COO^-NH_4^+$ surfactant at the CO_2|water interface at 318.15 K and average pressure of 23 MPa. For better visualization, a close-up of the interfacial region is shown.

selected scheme. In an approach where one fluid|fluid and two fluid|air interfaces are created (air|fluid|fluid|air), as in Dominguez and Berkowitz,[30] it becomes necessary to evaluate the surface tension of the pure liquids at the same thermodynamic conditions in order to calculate $\gamma_{C|W|S}$.

A time step of 2 fs was used. A cutoff of 10 Å was applied for the short range and real part of the Ewald summation. The Ewald sum was set to have a precision of 10^{-4}, and a convergence parameter of 0.244 $Å^{-1}$. The number of reciprocal vectors varied in all directions as a function of the size of the simulation box, while running in the NPT ensemble. The constrained bond lengths are handled with the SHAKE algorithm, with a precision of 10^{-5}. To allow some relaxation of the interfaces during equilibration, pressure was set to 20 MPa, with isotropic fluctuations in the simulation box size. Constant temperature and pressure was maintained by using the Nose-Hoover barostat and thermostat, with relaxation times of 0.5 ps. The system was initially equilibrated in the NPT ensemble at 318.15 K and 20 MPa for 500 ps. After the first equilibration period, a second equilibration for 500 ps was performed, now at constant total volume (NVT). Data collection for analysis proceeded in the NVT ensemble for the next 2.0 ns, with a total of 3.0 ns simulation time. The thermodynamic conditions in which the results are obtained during the last 2 ns are more conveniently described by *T*, *P*, and *A*. *T* is that of the set value of 318 K. The average interfacial area per molecule (*A*) is 84 $Å^2$. The observed experimental value for this system at 318 K and 28 MPa is 100 $Å^2$/molecule.[53] The pressure can be calculated as the trace of the pressure tensor matrix[61]

$$P = \left(\frac{p_{xx} + p_{yy} + p_{zz}}{3}\right) \tag{9}$$

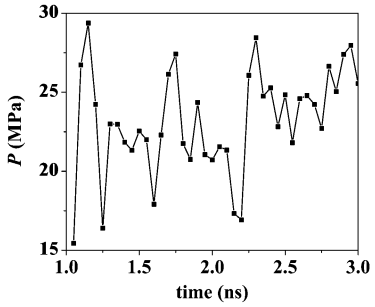

Figure 3. Block average pressure in 50 ps time-intervals, for the last 2 ns NVT production run. The average pressure $\langle P \rangle$ is 23.2 ± 3.3 MPa.

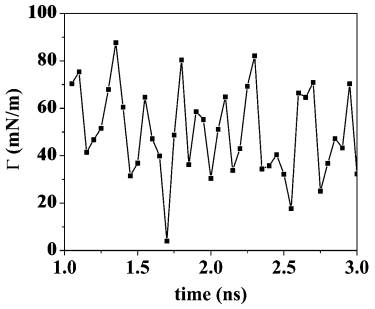

Figure 4. Block averages in 50 ps time-intervals for the total interfacial tension Γ (= $\gamma_{C|W} + \gamma_{C|W|S}$), for the last 2 ns of the simulation at 318 K and 23 MPa.

with $p_{\alpha\alpha}$ ($\alpha = x, y,$ or z) being the $\alpha\alpha$ element of the matrix. The block averages in 50 ps time intervals are shown in Figure 3. The line connecting the points serves as a guide to the eye. The average pressure $\langle P \rangle$ from the 2 ns simulation production run is 23.2 ± 3.3 MPa, which is close to the initial target of 20 MPa. Our previous experimental results indicate that the interfacial tension should have very low sensitivity to such small pressure variations in this pressure region, perhaps within experimental uncertainty.[49,53] A detailed description of the methods and parameters for the MD simulations described above can be found in the "The DL_POLY_2 User Manual".[60]

III. Results and Discussion

In this section, we present the results of the simulations and compare them to available experimental data, whenever possible. We also try to compare and contrast the C|W interface to the conventional O|W interface.

3.1. Interfacial Tension. The interfacial tension of the surfactant-modified C|W interface ($\gamma_{C|W|S}$) can be calculated with the knowledge of the binary C|W interfacial tension ($\gamma_{C|W}$) at the same conditions, through the following relationship:[30]

$$\Gamma = \sum_i \gamma_i = \gamma_{C|W|S} + \gamma_{C|W} \tag{10}$$

where *i* is the number of interfaces, which in our case is two: the bare and the surfactant-modified C|W interface. Γ, the total interfacial tension, can be obtained through the following relation:[51]

$$\Gamma = \left(p_{zz} - \frac{p_{xx} + p_{yy}}{2}\right) L_z \tag{11}$$

where L_z is the length of the simulation box in the *z* direction, normal to the interface. $\gamma_{C|W|S}$ can, therefore, be obtained by combining eqs 10 and 11. Figure 4 shows the evolution of Γ with time for the 2 ns simulation, where the block averages are

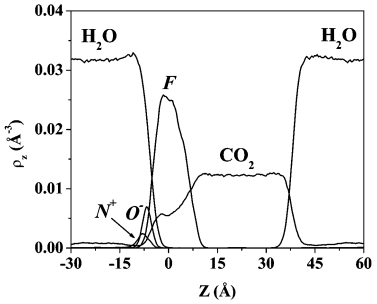

Figure 5. *Z*-dependent center of mass density profile for the CO_2|water interface at 318.15 K and 23 MPa. Note that there are two interfaces: one modified by the presence of surfactant molecules (to the left) and a binary CO_2|water interface (to the right). The surfactant tail-group is represented by the fluorine atom (F) profile, while the head-group and counterion are represented by the carboxylate oxygen (O^-) and the nitrogen (N^+) atomic density distributions, respectively.

connected with a line to facilitate visualization. The observed average of the blocks is 50 ± 19 mN/m. Subtracting the value of 33 ± 4 mN/m for $\gamma_{C|W}$ obtained at essentially the same conditions,[44] the resulting best estimate of $\gamma_{C|W|S}$ is 17 mN/m. The experimental values determined for the binary C|W interface and the C|W interface modified by the same PFPE−$COO^-NH_4^+$ surfactant at 318 K and at 27.6 MPa, are 22.0 and 3.0 mN/m, respectively.[53] While the calculated estimate of $\gamma_{C|W|S}$ differs significantly from the experimentally determined value, we observe that the calculated change of 17 mN/m in interfacial tension upon the addition of surfactant is in agreement with experiment, 19 mN/m. We conclude that the potential model for the amphiphile represents the experimentally observed influence of the PFPE surfactant on the C|W interface. Because the incorporation of added complexity such as the inclusion of explicit polarizability in the model does not seem to be a requirement for obtaining better quantitative agreement with experimental interfacial tension values,[30,62] we believe that quantitative agreement can most likely be improved via focus on the interaction parameters between CO_2 and water models, although there remain uncertainties in both experimental and calculated values.

3.2. Interfacial Profile. *3.2.1. General Characteristics.* To a large extent, the qualitative features observed for amphiphiles at conventional O|W interfaces is preserved for surfactants at the C|W interface, as can be observed by the *Z*-dependent density profiles relative to the box center-of-mass shown in Figure 5. The surfactant head-group is at the interface and completely submerged in the aqueous-rich phase, while the surfactant tail-group is mostly excluded from the aqueous phase. Nevertheless, water has some contact with the tail-group, as can be observed by the partial overlap of the water and fluorine profiles. The solvation of both head- and tail-group will be discussed in more detail below, in the context of radial distribution functions. It is also obvious from the density profiles in Figure 5 that CO_2 is capable of penetrating the surfactant tail region to a large extent, and to a much larger extent than is water. At the peak of the fluorine density distribution, the density of CO_2 is quite large, approximately 50% of its bulk value. This is notably larger than for CCl_4 in the hydrocarbon tail region of SDS surfactant at the CCl_4|W interface;[30] we estimate that value from Figure 1 of that reference to be approximately 30% of its bulk density. Furthermore, it is evident in Figure 5 that the CO_2 density decays relatively slowly as the tail region is penetrated farther toward the head-group. Significant CO_2 density is found even in the charged head-group region (O^-), in contrast to the comparable SDS|O|W system.[30] We emphasize

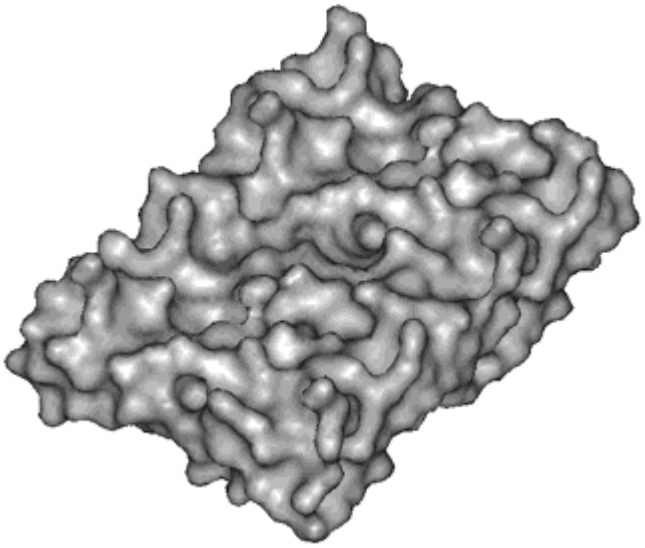

Figure 6. Snapshot of an equilibrium configuration of the CO_2|water interface (same configuration as in Figure 2) in the presence of surfactant molecules at 318 K and 23 MPa. The Connolly-like surface[65] shown is that of the water-rich side. It corresponds to a section of the system which was replicated nine times in the *x* and *y* directions, after the CO_2 and surfactant anions have been removed.

that such large penetration should not be viewed as arising due to the low surfactant coverage per se. On the contrary, the generally observed low surfactant coverage at the C|W interface has been attributed to the low free energy density difference of the binary C|W interface.[49] Obviously, other contributions, including those due to favorable CO_2−surfactant interactions, and the low cohesive energy density of fluorinated moieties (small tail−tail interaction), also have an impact on the observed density profile. It can be also observed that the NH_4^+ counterions are largely associated with the COO^- surfactant head-group, even though the presence of a tail in the profile for N^+ indicates that they can be occasionally also found away from the interfacial region. A similar trend is also seen for a monolayer of tetradecyltrimethylammonium bromide at the A|W interface.[27]

3.2.2. Interfacial Corrugation. Figure 5 also shows that the interfacial region containing the surfactant anions and counterions (to the left) is broadened compared to the binary C|W interface (to the right). Such an increase in interfacial width is expected since the presence of adsorbed surfactant reduces the interfacial tension as shown in Section 3.1. This relationship will be further discussed in the context of capillary-wave theory[63] later in this section. Such observation is in agreement with the computer simulations of Schweighofer et al.,[28] who observed a similar broadening behavior when adding SDS surfactant to the binary CCl_4|W interface. Capillary-wave theory predicts an inverse square-root dependence of the corrugations of the interface with interfacial tension. [64] Figure 6 is a representation of such corrugations. Figure 6 is analogous to, and can be directly compared to, Figure 6 of our previous investigation,[44] a study of the neat binary C|W interface. The only difference between the figures is that, in this work, not only CO_2 but also the surfactant molecules were removed for the construction of this Connolly-like surface,[65] which represents the corrugations as probed on the aqueous side of the interface. It can be clearly seen that the corrugations are enhanced when in the presence of amphiphiles compared to the binary EPM2 CO_2|SPC/E water interface (at the same temperature, and nearly identical simulation box size).[44]

3.2.3. Comparison with Hydrocarbon Systems: Experiments and MD. Certain microscopic structural information of the A|W

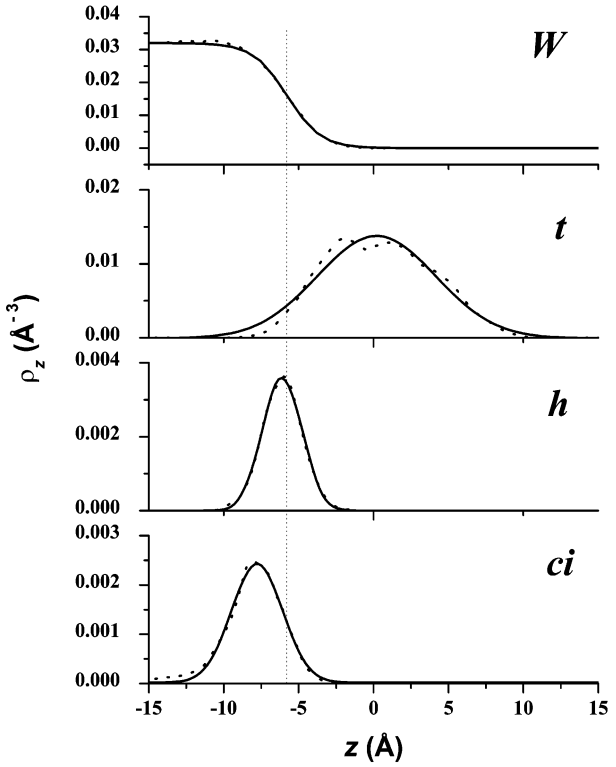

Figure 7. *Z*-dependent density profile at 318 K and 23 MPa. The dotted lines are the computed profiles and the continuous lines are their best fit (eqs 12 and 13), as described in the text. W stands for water, t for surfactant tail-group (C), h head-group (C^-), and ci counterion (N^+). Here, to represent the tail-group, we use the number density profile of the C atoms along the surfactant tail instead of the F distribution to facilitate comparison with previous investigations. Width and center of F distribution are given in the text.

and also O|W interfaces, including density profiles, can be experimentally probed by X-ray and neutron reflectivity; see, e.g., Lu et al.[8] Even though no such experimental information is available for the C|W interface at this time, the following detailed analysis of the profiles shown in Figure 5 and expanded in Figure 7 can serve as a guide for future experimental investigations. Furthermore, such an analysis can be used for comparing and contrasting this novel high-pressure C|W interface with conventional interfacial systems. Parameters such as the tail thickness, which can be deduced from the width of the tail profile, are of particular interest in microemulsion science. This follows from the fact that tail extension is a direct measure of the organization of the monolayer (tilt and defects).[66] The surfactant tail region, in turn, mediates the interaction between interfaces, thus directly influencing microemulsion stability.[67,68] The separations between the centers of component profiles also hold valuable information. For example, a direct correlation between the depth of penetration of the surfactant head-group into the water-rich phase and the number of gauche defects in the surfactant tail compared to alternative surfactants has been experimentally established.[16]

With that purpose in mind, we show in Figure 7 the *z*-dependent density profiles on an expanded scale for water (W) and for the surfactant head-group (h), counterion (ci), and tail (t). We also show their fit to tanh (water) and Gaussian (surfactant component) distributions, following Lu and co-workers.[69] The profile for water is fit to the following functional form:

$$\rho_w = \frac{1}{2} * \rho_w^0 \left[1 + \tanh\left(\frac{z - z_w^0}{w}\right)\right] \qquad (12)$$

TABLE 4: Widths (σ and w) and Separation Distance (δ) of the Fitted Profiles for the COO^- Head-group (h), Surfactant Tail-group (t), and Water (W) at 318 K, 23 MPa, and 84 Å²/molecule[a,b]

	σ_t (Å)	σ_h (Å)	w(Å)	δ_{tW} (Å)	δ_{hW} (Å)	δ_{ht} (Å)
PFPE|CO_2|W	11.2	3.7	2.2	6.0	0.3	6.30
SDS|CCl_4|W	10.4	4.1		4.9	1.4	6.30

[a] Parameters for SDS are for an isolated surfactant molecule at the CCl_4|W interface.[29] [b] Note that PFPE−COO^- and SDS surfactants have the same number of atoms in their backbone.

where z_w^0 is the center and w the width of the distribution. It is worth noticing that the thickness obtained by fitting the profile to an error function has been shown to be a better estimator of the interfacial order parameter.[70] However, a mathematical relationship between the widths obtained from tanh and erf is available.[70] The surfactant profiles are fit to a Gaussian distribution of the form

$$\rho_i = \rho_i^0 \exp\left[\frac{-4(z - z_i^0)^2}{\sigma_i^2}\right] \qquad (13)$$

where σ_i is the width of the distribution i ($i = h, ci, t$) and z_i^0 is the center. The profiles obtained from this work are represented by dashed lines, and the fits by continuous lines. The dotted line parallel to the *y*-axis in Figure 7 indicates the *z* position where the aqueous profile reaches half of its bulk density. The values for width and separation distances ($\delta_{iw} = |z_i^0 - z_w^0|$) are shown in Table 4. Here we use the number density profile of the C atoms along the surfactant tail instead of the F distribution shown in Figure 5. This is done to facilitate the comparison with previous investigations. However, the observed width and center of the F profile of 12.0 and 0.5 Å, respectively, are very similar to those of the C distribution (see Table 4). For comparison, the parameters obtained for an isolated SDS molecule at the CCl_4|W interface[29] are also shown in Table 4. We need to interpret the observations with care, however, given that δ_{hw} in Schweighofer et al.[29] includes both anion and counterion profiles as "head-group". Such an approach has the effect of bringing the position of the head-group profile more into bulk water.

It is interesting to observe that the PFPE−COO^- surfactant represents a thicker monolayer at the C|W interface compared to SDS at the CCl_4|W interface,[29] despite the fact that both have the same number of atoms in their hydrophobic backbone. As it will be discussed later, this behavior can be attributed only partially to the fact that the PFPE−COO^- monolayer is somewhat less tilted than the isolated SDS. We note that this comparison is valid since chain length and tilt for the SDS monolayer remain approximately constant on increasing surface coverage from the isolated chain to 45 Å²/molecule.[29,30] Another interesting aspect to observe is that the PFPE−COO^- surfactant penetrates deeper into CO_2 compared to SDS in CCl_4, as indicated by the separation between the center of the tail- and head-group profile to the center of the water distribution (δ_{ij}). Besides the more hydrophobic nature of the tail, another possible contribution to the observed separation distances can arise due to the favorable enthalpic interaction between CO_2 and the fluorinated tail-group. As pointed out by Conboy and co-workers,[16] a possible implication of such behavior is the increase in the probability for gauche defects in the surfactant tail-group, compared to alternative surfactants. This is related to the fact that the "conformational fluidity" of the tail-group is increased when it is drawn farther from the aqueous phase.[16]

The widths (σ_i and w) can also be compared to experimental information derived from the self-partial structure factors from neutron reflectivity, and the relative separation distances between the center of the distributions (δ_{ij}) can be compared to the information contained in the cross species partial structure factors.[69] To compare the widths from MD to the experimentally observed values, however, a correction due to the presence of increased thermal roughness,[8] which is not fully accounted for in the simulations due to the system's small size[27] and periodic boundary conditions,[24] needs to be computed. Here we employ a correction as proposed by Schlossman and co-workers[71] to derive the expected experimental value:

$$\sigma^2_{\text{exptl}} = \sigma_{\text{MD}}{}^2 + \sigma_{\text{corr}}{}^2 \tag{14}$$

It is generally accepted[71] that the experimentally determined width of fluid−fluid interfacial systems (σ_{exptl}) has an intrinsic component (σ_o) due to the small but finite mixing of fluid phases, and a component due to thermal excitation of interfacial fluctuations (σ_{cap}). Implicit in eq 14 is the assumption that the results from computer simulations (σ_{MD}) include the contribution due to this intrinsic width (σ_o), and also that from the part of the excitation spectrum that appears in the experimentally observed result (part of σ_{cap}).[70] Hence, σ^2_{corr} accounts for the difference in σ^2_{cap} not accounted for in our small system. From capillary-wave theory,[63] the interfacial broadening is expressed in terms of the interfacial tension and the temperature of the system. It also contains a system-size dependence as illustrated in the capillary-wave equation below:[72]

$$\langle \sigma^2_{\text{cap}} \rangle = \frac{k_b T}{2\pi\gamma} \ln\left[\frac{q_{\text{max}}}{q_{\text{min}}}\right] \tag{15}$$

where $\langle \sigma_{\text{cap}} \rangle$ is the width due to thermal fluctuations, and T and k_b have the usual meaning. The low wave-vector (large wavelength) limit $q_{\text{min}} = 2\pi/L$ is system size-dependent, and the large wave-vector limit, $q_{\text{max}} = 2\pi/l$, is determined by either the molecular correlation length or the molecular size ($l \sim 5-10$ Å).

When calculating the correction term from eq 15, σ^2_{corr}, however, we take $q_{\text{max}} = 2\pi/L_x$, where $L_x = A^{1/2}$ is the size of the cross sectional area of the simulation box (25.82 Å), and $q^{\text{exptl}}_{\text{min}}$ of $2\pi/10^5$ Å.[71] From our early experimental work, the estimated γ at the cμc at 45 °C and 28 MPa is 3 mN/m.[53] Plugging in this value for γ, with the above wave-vector limits, σ_{corr} is 13.3 Å. Adding (eq 14) σ_{corr} to our MD simulations results for σ_t and w, the expected experimental value for the thickness of the PFPE−COO^- surfactant tail-group and water profile at the C|W interface are ∼17 and 13 Å, respectively. For comparison, on a curved W|C microemulsion interface, the thickness of the PFPE−COO^- tail-group (including thermal fluctuations) as determined by SANS with an ad hoc density profile varies from 12 to 17 Å, in a pressure−temperature range of ∼10−38 MPa and 288−353 K.[42]

To compare and contrast our study to a conventional O|W system, we use the experimental results of Lu and co-workers.[8] In their work, the reported thickness, including thermal fluctuations, for a $C_{12}E_5$ (pentaethylene glycol monododecyl ether) surfactant monolayer at the dodecane|W interface, is 20 Å, slightly higher than the PFPE monolayer (same number of carbons in the backbone) at the C|W interface. Note, however, that in their case the surfactant interfacial density is approximately twice as large. The observed thickness for the water profile is 8.5 Å,[8] which is much smaller than the corrected value for our system. Interestingly, Lu et al. report that the thickness of the water density profile is the same with and without dodecane present, implying a negligible change in interfacial tension when decane is added to the surfactant monolayer initially at the A|W interface. In our case, however, the interfacial free energy changes significantly (large reduction in the experimental value of the interfacial tension) when comparing a PFPE−COO^- monolayer at the A|W and at the C|W interface.[53,73] The surface tension for the PFPE−NH_4^+ surfactant at the same surface coverage and a similar temperature of 298 K can be estimated from the surface tension vs surfactant concentration isotherm,[74] with the help of a surface equation of state.[49] This value is estimated to be between 52 and 64 mN/m, depending on the actual dissociation of the carboxylic headgroup. This is significantly different from the experimental value of 3 mN/m experimentally obtained for the PFPE−NH_4^+ at the C|W interface at 318 K and 23 MPa.[53]

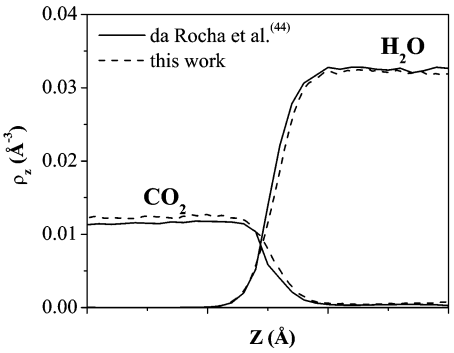

Figure 8. Comparison of the center of mass density profile for the bare CO_2|water interface obtained in this work, with the interfacial profile for the same potential models and nearly identical thermodynamic conditions obtained in our earlier study.[44]

In considering the validity of such comparisons between experiments and computer simulations, it is worth noticing that γ calculated from eq 15, using values of $\langle \sigma^2 \rangle$ from fits of the aqueous number density profile of MD simulations, agrees quantitatively with the independent values calculated from the pressure tensor and also with the experimental values (see, e.g., Senapati and Berkowitz[75]). We conclude, therefore, that even at such small dimensions, the computer simulations are capable of probing satisfactorily the capillary waves due to thermal fluctuations. Moreover, it follows that the capillary wave contribution dominates the total $\langle \sigma^2 \rangle$ value from MD, with a negligible contribution from the intrinsic thickness. While this seems to be true for small molecule interfaces such as CCl_4|W,[75] a small correction term has been proposed for higher alkanes (above C_6).[71]

3.2.4. Interfacial Correlation. An important question regarding the simulation methodology concerns possible correlations between the two interfaces present in our system, namely, the binary C|W and the C|W|surfactant interface. These might arise due to the imposed periodic boundary condition in the direction perpendicular to the interface (z). To answer this question, we compare the density profiles of the binary C|W interface obtained in this work and the one obtained in our earlier investigation of the neat C|W interface, at nearly identical thermodynamic conditions.[44] The close agreement between the profiles shown in Figure 8 is a strong indication that the methodology employed here is a suitable one.

3.3. Molecular Description of the Interfacial Region. *3.3.1. PFPE Tail-group. Carbon Atom Profiles.* A more detailed description of the surfactant tail-group at the interfacial region can be obtained from the number density distribution of the

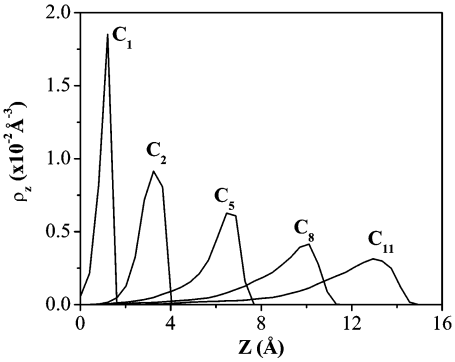

Figure 9. Number density profiles of the carbon atoms of the surfactant tail-group relative to the head-group C^- in the direction normal to the interface. The curves are labeled according to Table 3. The leftmost curve corresponds to the CF2 carbon (C_1) adjacent to the carboxylic carbon (C^-), while the rightmost curve corresponds to the CF3 carbon (C_{11}) farthest from the head-group. C_2, C_5, and C_8 are corresponding carbons in the three repeat units.

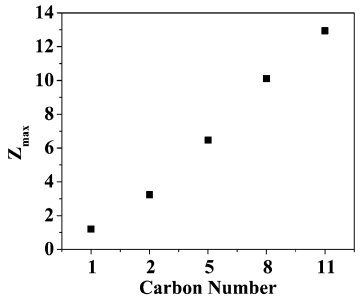

Figure 10. Center of mass coordinate at the peak of the number density profile (Z_{max}) of the carbon atoms in the surfactant tail-group shown in Figure 9.

carbon atoms along the surfactant backbone, as shown in Figure 9. To account for the fact that different surfactants can have their carboxylate head-groups at different *z*-positions due to the rough nature of the interface, the profiles are accumulated relative to the *z*-coordinate of each respective carboxylate carbon. The profiles are useful in understanding the degree of organization of the monolayer, and the effect of solvation by CO_2. Note the carbon numbers follow the same labels as in Table 3. The profile for C_1, the CF2 carbon adjacent to the carboxylate head-group, is shown in the leftmost curve, while C_{11}, the CF3 carbon farthest from the head-group, is shown in the rightmost curve. The profiles for three corresponding carbons in consecutive repeat units, which have a CF3 pendant group attached to them, are also shown.

For a collapsed monolayer, e.g., in the case of a poor solvent, one would expect profiles that overlap with each other significantly. The reverse can be expected for a well-solvated and/or compressed monolayer. The profiles in Figure 9 clearly become broader and start overlapping as the atom carbon number increases—going away from the head-group. This is expected since there is a larger configurational space available to each segment as one goes farther toward the end of the tail. However, only the tails of the profiles overlap. Moreover, the individual distributions change smoothly and are nearly equally spaced relative to the surface normal. Figure 10 shows the linearity explicitly. Because of the relative low surface coverage, we can infer that the nature of the profiles is related to good solvation of the surfactant tails by CO_2, since otherwise the tails would collapse to fill the interface. We will elaborate further on the solvation of the surfactant fluorinated tail-group by CO_2 in the context of radial distribution functions, below.

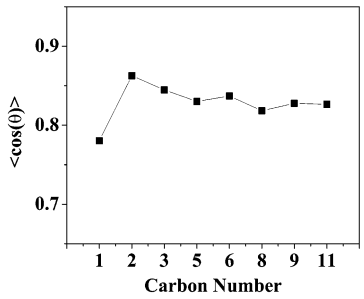

Figure 11. The cos of the angle formed between the vector normal to the interface and the vector connecting C^-C_i, as a function of the carbon number in the surfactant tail-group. Carbon atoms labeled as in Table 3.

Monolayer Thickness and Tilt. A good estimate of the surfactant monolayer thickness is obtained by calculating the difference in Z_{max} between C_1 and C_{11}, which is found to be 10.9 Å. This value, plus the projection of the bond distance between C_1 and C^- (see Table 2 and Figure 11) results in a total of 11.9 Å, which compares very well with the time average thickness value $\langle lz \rangle$ of 11.7 Å, the projection of the vector connecting C^- to C_{11} onto the *z* direction. It is also in very good agreement with the calculated Gaussian width of 11.2 Å. This represents a monolayer that is approximately 3 Å more extended than that calculated for SDS at the CCl_4|W interface.[30] It is also thicker than calculated for a monolayer of a hydrocarbon surfactant with 14 carbons (tetradecyltrimethylammonium bromide) at the A|W interface.[27] The average value of the magnitude of the vector connecting the carboxylate carbon to the CF3 carbon at the end of the surfactant tail-group $\langle l \rangle$ is 14.1 Å, which is significantly more extended than the value for the gas-phase optimum configuration of 12.5 Å.

The tilt of the surfactant monolayer with respect to the interfacial normal, which is also an estimator of the organization of the monolayer, can be calculated from $\langle \theta \rangle = \langle a \cos(lz/l) \rangle$. The angle of 34° found in this work is somewhat smaller than the tilt obtained for SDS at the CCl_4|W interface of 39° at both infinite dilution[29] and at 45 Å^2/molecule.[30] While Berkowitz and co-workers observed a change in tilt from 47 to 39° upon adding CCl_4 to a SDS monolayer initially at the A|W interface,[29,30] neutron reflectivity experiments suggest that the tilt of a $C_{12}E_5$ monolayer (same number of atoms in the backbone as SDS and the PFPE in this work) changes from 40° (A|W) to approximately 0° (O|W) (vertical) upon the addition of a layer of dodecane.[8] The experimentally observed result for the tilt of $C_{12}E_5$ monolayer at the A|W interface[8] is close to the tilt calculated for SDS at the A|W interface.[29,30] The vertical alignment when in the presence of dodecane is, however, in striking difference to the findings in Berkowitz'[30] and this work. Although the system is not the same, this discrepancy could be an artifact due to the experimental methodology and/or model employed by Lu and co-workers.[8] Due to experimental limitations, only a thin layer of dodecane is deposited on the surfactant monolayer, creating a water/surfactant−oil/air interface, instead of a full bulk oil layer. Another possible and more likely source for the observed difference is the underlying assumptions used in the calculation of $\langle \theta \rangle$. A zero defect chain is assumed for calculating *l*, and *lz* is found on the basis of the hypothesis that there is no change in the capillary width when the dodecane layer is added to the $C_{12}E_5$ monolayer at the A|W interface.

On the basis of the above discussion, one can conclude that the PFPE monolayer at the C|W interface has an overall level of organization comparable or better than conventional O|W systems. It is worth noticing that while Dominguez and

Berkowitz observed no effect of surface coverage on $\langle\theta\rangle$ or $\langle lz\rangle$ on their computer simulation study of the SDS monolayer at the CCl_4|W interface,[30] Lu and co-workers[66] have shown that for a C_{16}TAB surfactant monolayer at the A|W interface there is a one-to-one relation between layer thickness and surface coverage. Because the main contribution to the thickness is expected to be the monolayer tilt,[66] they conclude that as the *A* increases (or coverage decrease), so does $\langle\theta\rangle$. It is therefore a striking result that the overall degree of organization and thickness of the monolayer investigated in this work is similar to that of SDS at the CCl_4|W interface, with the latter at approximately twice the coverage. One might attribute such behavior to the possibly higher stiffness of the PFPE surfactant tail due to the presence of the large F atoms and the pendant CF3 groups. However, whereas increased steric hindrance is to be expected, the presence of the ether linkages increases the tail flexibility significantly, as will be further discussed below.[76] Moreover, on the basis of the discussion above, a higher incidence of gauche defects would be expected for tails that are centered farther away from the water-rich phase, compared to alternative surfactants.[16] Therefore, we are led to the conclusion that favorable attractive interactions between CO_2 and the fluorinated tail region are playing a marked role in the observed organization and tail conformation.

The cos of the angles formed between the vector connecting the carboxylic carbon to the carbon atoms along the surfactant backbone (C^-−C_i) and the vector normal to the interface $\langle\cos\theta\rangle$ are shown in Figure 11. The line connecting the points is used simply as a guide to the eye. For clarity, the $\langle\cos\theta\rangle$ involving the pendant C atoms are not shown. All carbon atoms in the PFPE backbone are found to assume an average orientation closer to the surface normal than those for SDS at the CCl_4|W interface.[30] Analogous to the trend for the SDS at the CCl_4|W interface, a plateau in $\langle\cos\theta\rangle$ is reached toward the end of the surfactant tail, with $\langle\cos\theta\rangle$ C−C_{11} in agreement with the calculated tilt cited above.

Order Parameter. A better estimator of the orientational order of the surfactant chains in the monolayer is the fluorine order parameter (S_{CF}) defined in eq 16:

$$S_{CF} = \frac{3}{2}\langle\cos\theta^2\rangle - \frac{1}{2} \qquad (16)$$

This is a definition analogous to that of the deuterium order parameter S_{CD}, which can be experimentally determined from the residual quadrupole splitting in NMR.[77] Here, θ is the angle between the vector connecting C_i−F and the normal to the interface. The brackets indicate time average, in this case over a 2 ns time interval. A value of −0.5 for S_{CF} indicates that the C_i−F bond is perpendicular to the interface normal. S_{CF} is 1 for bonds parallel to the interface and 0 for an isotropic distribution. The S_{CF} for the PFPE surfactant tail-group is shown in Figure 12. A line connecting the points is used to guide the eye. For clarity, we report the values for the CF2 carbon next to the head-group, the CF3 at the end of the tail-group, and the other three corresponding carbons in consecutive repeat units—those with the attached CF3 pendant group.

It is evident from Figure 12 that chain anisotropy increases toward the end of the surfactant tail-group, in agreement with the profiles shown in Figure 9. A similar trend is seen for SDS at the CCl_4|W interface.[30] This is in contrast to more ordered monolayers, such as lipid bilayers in the crystalline phase, in which a plateau in S_{CD} extends through most of the phospholipid tail.[77] The values for S_{CF} in Figure 12 also indicate that the PFPE monolayer at the C|W interface has a higher degree of order than SDS at the CCl_4|W interface,[30] again despite the fact that the surface coverage is half that of SDS.

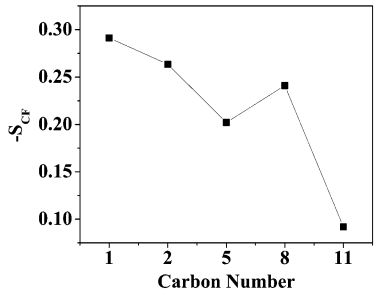

Figure 12. Order parameter (−S_{CF}; eq 16) as a function of the atom carbon number in the surfactant tail-group. Carbon atoms labeled as in Table 3. For better visualization, analogous to Figure 9, S_{CF} is shown for the bonds in the CF2 adjacent to the head-group, CF3 at the end of the surfactant backbone, and only three other corresponding carbons (C_2, C_5, C_8, with pendant CF3 groups) from sequential repeat groups.

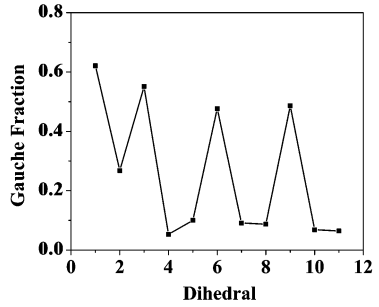

Figure 13. Fraction of gauche defects as a function of the dihedral angle. The first dihedral is that of O_1−C_1−C^-−O^- (see Table 3), and are thereafter sequentially numbered toward the opposite end of the surfactant backbone.

Gauche Defects. The average fraction of gauche defects is shown in Figure 13. The dihedrals under consideration start from the head-group—number 1, which includes the carboxylic and the CF_2 carbon as the central atoms −O−C_1−C^-−O^-, and are thereafter sequentially numbered toward the opposite end of the surfactant tail (see Table 3). The general features of Figure 13 result from a balance between the steric crowding due to the replacement of the small H by the larger F atoms,[78] and the presence of the pendant CF_3 groups, and an enhanced flexibility due to the presence of the ether linkages to the perfluorinated chain.[76] As reported by Smith and co-workers,[76] perfluoropoly(oxyethylene) has considerably higher flexibility than its hydrocarbon analogue, while perfluorination of linear hydrocarbons exerts the opposite effect. The dihedrals 3, 6, and 9, which involve a central C atom that has a pendant CF3 group and that participate in an ether linkage, present a high gauche fraction. The population of defects in the remainder of the surfactant backbone is reduced significantly, to less than 10%. This is significantly smaller than the ∼20−30% observed for SDS at the CCl_4|W interface. It is, however, larger than the nearly zero defect probability of higher surface coverage films including perfluorinated alkane monolayers[79] and partially fluorinated bilayers,[80] also obtained from MD simulations.

Tail Solvation. An important part of the microscopic characterization of the surfactant region consists of understanding the solvent−solute interaction. This characterization is especially important for the CO_2-tail side of the interface where very little microscopic information is available,[48] and where questions regarding the CO_2 solvation capacity are of major concern in surfactant-stabilized colloidal domains dispersed in bulk CO_2.[42,81,82] A clear picture of the structure of the solvent molecules around the surfactant tail-group can be obtained by

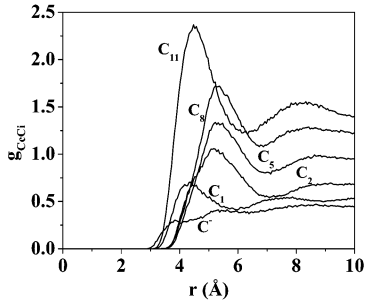

Figure 14. Radial distribution function between the C atom in CO_2 (C_c) and those along the surfactant backbone (C_i). Labels follow those in Table 3. *g* is normalized as described in the text.

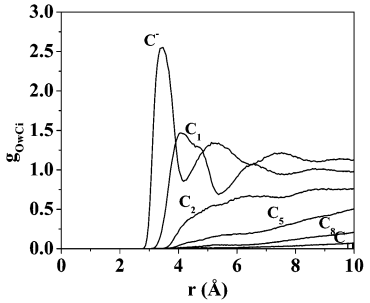

Figure 15. Radial distribution function between water molecules (O_w) and the C atoms along the surfactant backbone (C_i). Labels follow those in Table 3. *g* is normalized as described in the text.

determining the radial distribution function (RDF) between the carbon atom of CO_2 (C_c) and those carbon atoms along the surfactant backbone (C_i), denoted $g_{C_cC_i}$. All RDFs are normalized by the particle number density $\rho_i = N_i/V_{box}$; for the case of g_{CcCi}, we use ρ_{CO_2}. Such distributions, labeled by carbon atom number *i* according to Table 3, are shown in Figure 14. The intensity and relative sharpness of the first peak and first minimum of the distributions are evidence of the existence of structured CO_2 molecules around the surfactant tail-group. The ratio between the height at the first maximum (Δ_1) to that at the first minimum (Δ_2) of an RDF is an indicator of the resolution of the first solvation shell. Despite the fact that the peak intensities decrease toward the surfactant head-group due to a reduction in the CO_2 number density, the Δ_1/Δ_2 ratio remains approximately constant, with a small increase from C8 to C2, with C2 having the same ratio as C11. This is a strong indication that the surfactant tail is well solvated by CO_2 throughout. Even the head-group C^- is significantly solvated by CO_2, as noted earlier (see Figure 5). Such behavior is of relevance in the context of microemulsion stability, where strong solvent−tail interactions are required to balance the destabilizing attractive interactions between the tail segments of different droplets.[67]

Water Penetration in the Monolayer. We noted earlier that water did not tend to penetrate the surfactant tail region. The $g_{O_wC_i}$ profiles shown in Figure 15 clearly show that even though water solvates the carboxylic head-group, and is present to a large extent near the CF2 adjacent to it, very little contact exists between water and the remainder of the hydrophobic surfactant tail. An important contribution to the small but finite values for $g_{O_wC_i}$ arises due to the corrugations of the interface; the head-groups do not lie in a plane. Similar results have been observed for surfactant monolayers at the A|W interface, by MD and neutron reflectivity.[13,24] In agreement with these results, appreciable water contact determined by ^{19}F NMR in reverse micelles of a perfluorinated surfactant ($CF_3(CF_2)_6COONa$) is detected only up until the first CF2 adjacent to the head-group.[83]

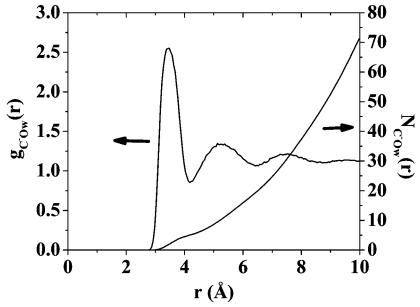

Figure 16. Head-group (C^-)−water (O_w) radial distribution function ($g_{C^-O_w}$) and number of water neighbors around a central head-group ($N_{C^-O_w}$). *g* is normalized as described in the text.

3.3.2. Carboxylate Head-group and the Ammonium Counterion. We have shown experimentally in the past that the dominating driving force for aggregation of the anionic PFPE−$COO^-NH_4^+$ in bulk CO_2 in the presence of water is the favorable enthalpic interaction between head-group and water.[49] Correspondingly, the nature of the counterion and its interaction with the head-group can play a major role in the self-assembly process both in normal and reverse systems.[84] For example, structural transitions of surfactant aggregates can be accomplished by varying type and concentration of the counterion.[84] It is, therefore, of great relevance to understand head-group solvation and the interaction between head-group and counterion. It is worth noting, however, that, in general, surfactant head-groups will experience reduced electrostatic repulsion in reverse microemulsions formed in bulk CO_2, compared to conventional systems, due simply to the typically much smaller surfactant surface coverage generally observed at the C|W interface.[49]

Head-group Solvation. The RDF between the carboxylate carbon and the water oxygen ($g_{C^-O_w}$) is shown in Figure 16. As expected, the plot reveals a very structured solvent region around the head-group, with a well-defined first and broader second solvation shell. The position and sharpness of the first peak in $g_{O^-H_w}$ (not shown), are very similarly to simulated results for $HCOO^-$ and H_3CCOO^-.[58] With a first minimum at 4.1 Å, the observed number of water neighbors (O_w) around the head-group (C^-) in its first solvation shell N_{C-O_w} is 5.0 These results compare very well with previous investigations of small $HCOO^-$ and H_3CCOO^- anions in TIP4P water,[58] where an $N_{C^-O_w}$ of 7.3 and 6.6 water molecules is calculated around the formate and acetate anions, respectively, with a first minimum also at approximately 4.1 Å.[58] For a single sodium octanoate surfactant in bulk SPC/E water,[85] the carboxylate head-group has a hydration number of 7.9 (hydration number defined as the number of water molecules with O_w within 4.25 Å from the carboxylate oxygen). This number is found to be only slightly reduced upon micellization.[85] Due to the presence of NH_4^+ counterions, which, as will be shown below, form ion-pairs with the head-group, there is additional reduction in $N_{C^-O_w}$ in the present case.

Head-group Association with the Counterion. An estimation of the degree of association between head-group and counterions can be obtained by the ratio between the number of counterions ($N_{C^-N^+}$) to the number of head-groups ($N_{C^-C^-}$) belonging to the first solvation shell of a head-group. Figures 17 shows the carboxylate counterion RDF and the running number of neighbor ions. The $g_{C^-C^-}$ and $N_{C^-C^-}$ are not shown. The estimated neutralization of the head-group is ∼88%. This value is in agreement with the NH_4^+ profile shown in Figure 5 (note a tail in the N^+ profile extending into bulk water), and with the observation that there is, in general, one in eight counterions

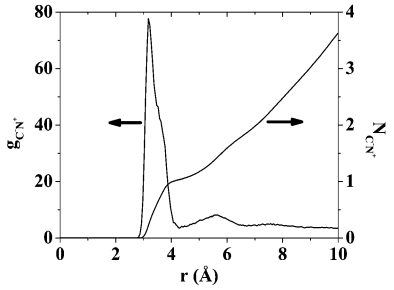

Figure 17. Head-group (C^-)−counterion (N^+) radial distribution function ($g_{C^-N^+}$) and number of counterions neighbors around a central head-group ($N_{C^-N^+}$). *g* is normalized as described in the text.

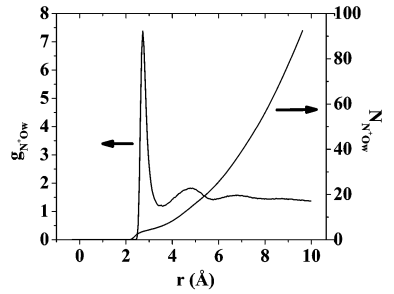

Figure 18. Counterion (N^+)−water (O_w) radial distribution function ($g_{N^+O_w}$) and number of water molecules around a central counterion ($N_{N^+O_w}$). *g* is normalized as described in the text.

that is solvated in bulk water. The experimentally estimated neutralization fraction of ionic surfactants in micelles, using SANS, is found to vary roughly from ∼0.5 to 0.8, and is significantly affected by the type of counterion. [86] No direct correlation between the size of the counterion and the micellar fractional charge is, however, observed.[86] More recently, Su and co-workers,[13] using neutron reflectivity, inferred that while approximately 15% of the tetramethylammonium ions penetrate the head-group region, 63% form a 16 Å-thick layer (obviously not all of them ion-pairing) below a DS monolayer at the A|W interface. For reverse micelles in bulk CO_2, MD simulations with a dichain $(C_7F_{15})(C_7H_{15})CHSO_4^-$ anion and a smaller Na^+ counterion indicate ∼75% association.[48]

Counterion Solvation. The counterion water interaction is reflected in the RDF shown in Figure 18 for $g_{N^+O_w}$. The very intense first peak at 2.8 Å is characteristic of hydrogen-bonding with water molecules. The first solvation shell around the NH_4^+ counterion is well defined, with a calculated $N_{N^+O_w}$ of ∼5 water molecules, followed by a broader second shell. While the peaks and general features of the distribution are similar to those obtained for NH_4^+ in bulk water,[58] we observe a significant reduction in the Δ_1/Δ_2 ratio and $N_{N^+O_w}$ (compare to 5.7) for the first solvation shell, and a much less evident second shell. This is a direct consequence of forming ion-pairs with the surfactant head-group.

IV. Conclusions

This work has presented a detailed microscopic and quantitative description of the structure of a PFPE−$COO^-NH_4^+$ surfactant monolayer at the high-pressure CO_2|water interface. Despite the fact that the system has the relatively low surface coverage generally observed for water-in-CO_2 microemulsion-forming amphiphiles,[49] the results obtained here indicate that the monolayer has a very similar degree of order to hydrocarbon surfactants adsorbed at the O|W interface.[29,30]

The features of the carbon atom profiles in the PFPE backbone consistently indicate a fairly organized and extended chain monolayer. The monolayer thickness, estimated from the width of the tail profile, the projection in the *z* direction of the vector connecting the head-group and the terminal surfactant carbon, and the position of the last peak of the carbon atom profile, relative to the head-group, are all in agreement. The resulting value of about 12 Å represents a somewhat thicker monolayer than a corresponding hydrocarbon surfactant (with the same number of atoms in the backbone) at the oil|water interface,[30] and also thicker than that for a surfactant with a C_{16} moiety at the air|water interface.[27] This result can be only partially explained by the smaller average tilt of the PFPE monolayer. We suggest that the favorable CO_2−fluorinated tail interactions also play a significant role in the observed result. The results from atomistic density distributions and from the RDFs between CO_2 and those sites along the surfactant backbone also corroborate the idea that CO_2 is a good solvent for the PFPE tail. Water is essentially excluded from the tail region, in accord with experiment.[83] Note that while steric crowding due to the F atoms and CF3 pendant groups can increase tail extension, the presence of ether linkages enhance its flexibility,[76] as evident in the calculated fraction of gauche defects. The calculated thickness, in fact, compares well with the upper bound found for the same amphiphile and an ad hoc model for the density profile at the curved C|W interface,[42] when corrected due to the thermal fluctuations of the interface.

Future work will consider the analysis of the solvent capacity of CO_2 for fluorinated surfactant tails. Specifically, we will consider alternative solvent models, including the air|water interface. In addition, comparative simulations for alternative fluorocarbon surfactants and candidate hydrocarbon surfactants are of great interest.

Acknowledgment. This material is based upon work supported in part by the STC Program of the National Science Foundation under Agreement No. CHE-9876674. Additional support has been provided by the R. A. Welch Foundation.

References and Notes

(1) Fendler, J. H. *Membrane Mimetic Chemistry*; John Wiley & Sons: New York, 1982.

(2) Shah, D. O. *Micelles, Microemulsions, and Monolayers: Quarter Century Progress at the University of Florida*; Shah, D. O., Ed.; Marcel Dekker: New York, 1998; pp 1−52.

(3) Ulman, A. *Introduction of Ultrathin Films, from Langmuir−Blodgett Films to Self-Assembly*; Academic Press: Boston, MA, 1991.

(4) Roberts, G. *Langmuir−Blodgett Films*; Plenum Press: New York, 1990.

(5) Miranda, P. B.; Shen, Y. R. *J. Phys. Chem. B* **1999**, *103*, 3292−3307.

(6) Schreiber, F. *Prog. Surf. Sci.* **2000**, *65*, 151−256.

(7) Penfold, J.; Richardson, R. M.; Zarbakhsh, A.; Webster, J. R. P.; Bucknall, D. G.; Rennie, A. R.; Jones, R. A. L.; Cosgrove, T.; Thomas, R. K.; Higgins, J. S.; Fletcher, P. D. I.; Dickinson, E.; Roser, S. J.; McLure, I. A.; Hillman, A. R.; Richards, R. W.; Staples, E. J.; Burgess, A. N.; Simister, E. A.; White, J. W. *J. Chem. Soc., Faraday Trans.* **1997**, *93*, 3899−3917.

(8) Lu, J. R.; Li, Z. X.; Thomas, R. K.; Binks, B. P.; Crichton, D.; Fletcher, P. D. I.; McNab, J. R.; Penfold, J. *J. Phys. Chem. B* **1998**, *102*, 5758−5793.

(9) Thoma, M.; Schwendler, M.; Baltes, H.; Helm, C. A.; Pfohl, T.; Riegler, H.; Mohwald, H. *Langmuir* **1996**, *12*, 1722−1728.

(10) Staples, E.; Penfold, J.; Tucker, I. *J. Phys. Chem. B* **2000**, *104*, 606−614.

(11) Li, Z. X.; Lu, J. R.; Fragneto, G.; Thomas, R. K.; Binks, B. P.; Fletcher, P. D. I.; Penfold, J. *Colloids Surf., A−Physicochemical and Engineering Aspects* **1998**, *135*, 277−281.

(12) Conboy, J. C.; Messmer, M. C.; Richmond, G. L. *J. Phys. Chem.* **1996**, *100*, 7617−7622.

(13) Su, T. J.; Lu, J. R.; Thomas, R. K.; Penfold, J. *J. Phys. Chem. B* **1997**, *101*, 937−943.

(14) Gragson, D. E.; Richmond, G. L. *J. Phys. Chem. B* **1998**, *102*, 569−576.

(15) Gragson, D. E.; Richmond, G. L. *J. Phys. Chem. B* **1998**, *102*, 3847−3861.
(16) Conboy, J. C.; Messmer, M. C.; Walker, R. A.; Richmond, G. L. *Prog. Colloid Polym. Sci.* **1997**, *103*, 110−120.
(17) Conboy, J. C.; Messmer, M. C.; Richmond, G. L. *Langmuir* **1998**, *14*, 6722−6727.
(18) Shelley, J. C.; Shelley, M. Y. *Curr. Opin. Colloid Surf. Sci.* **2000**, *5*, 101−110.
(19) Maple, J. R. *Force Fields: A General Discussion*; von Rague Schleyer, P., Ed.; John Wiley & Sons Ltd: Chichester, U.K., 1998; Vol. 2, pp 1015−1024.
(20) Allinger, N. L. *Force Fields: A Brief Introduction*; von Rague Schleyer, P., Ed.; John Wiley & Sons Ltd: Chichester, U.K., 1998; Vol. 2, pp 1013−1015.
(21) Karaborni, S.; Toxvaerd, S.; Olsen, O. H. *J. Phys. Chem.* **1992**, *96*, 4965−4973.
(22) Pohorille, A.; Benjamin, I. *J. Phys. Chem.* **1993**, *97*, 2664−2670.
(23) Kuhn, H.; Rehage, H. *J. Phys. Chem. B* **1999**, *103*, 8493−8501.
(24) Bocker, J.; Schlenkrich, M.; Bopp, P.; Brickmann, J. *J. Phys. Chem.* **1992**, *96*, 9915−9922.
(25) Bandyopadhyay, S.; Tarek, M.; Lynch, M. L.; Klein, M. L. *Langmuir* **2000**, *16*, 942−946.
(26) Okamura, E.; Fukushima, N.; Hayashi, S. *Langmuir* **1999**, *15*, 3589−3594.
(27) Tarek, M.; Tobias, D. J.; Klein, M. L. *J. Phys. Chem.* **1995**, *99*, 1393−1402.
(28) Schweighofer, K. J.; Essmann, U.; Berkowitz, M. *J. Phys. Chem. B* **1997**, *101*, 10775−10780.
(29) Schweighofer, K. J.; Essmann, U.; Berkowitz, M. *J. Phys. Chem. B* **1997**, *101*, 3793−3799.
(30) Dominguez, H.; Berkowitz, M. L. *J. Phys. Chem. B* **2000**, *104*, 5302−5308.
(31) Kuhn, H.; Rehage, H. *Colloid Polym. Sci.* **2000**, *278*, 114−118.
(32) Jacobson, G. B.; Lee, C. T.; da Rocha, S. R. P.; Johnston, K. P. *J. Org. Chem.* **1999**, *64*, 1207−1210.
(33) Johnston, K. P.; Harrison, K. L.; Clarke, M. J.; Howdle, S. M.; Heitz, M. P.; Bright, F. V.; Carlier, C.; Randolph, T. W. *Science* **1996**, *271*, 624−626.
(34) Beckman, E. J. *Science* **1996**, *271*, 613−614.
(35) Kane, M. A.; Baker, G. A.; Pandey, S.; Bright, F. V. *Langmuir* **2000**, 2000, 4901−490.
(36) Holmes, J. D.; Steytler, D. C.; Rees, G. D.; Robinson, B. H. *Langmuir* **1998**, *14*, 6371−6376.
(37) Ji, M.; Chen, X.; Wai, C. M.; Fulton, J. L. *J. Am. Chem. Soc.* **1999**, *121*, 2631−2632.
(38) Holmes, J. D.; Bhargava, P. A.; Korgel, B. A.; Johnston, K. P. *Langmuir* **1999**, *15*, 6613−6615.
(39) O'Shea, K.; Kirmse, K.; Fox, M. A.; Johnston, K. P. *J. Phys. Chem.* **1991**, *95*, 7863.
(40) Saito, S. *J. Supercrit. Fluids* **1995**, *8*, 117−204.
(41) McHugh, M. A.; Krukonis, V. J. *Supercritical Fluid Extraction: Principles and Practice*, 2nd ed.; Butterworth: Stonham, MA, 1994.
(42) Lee, C. T., Jr.; Johnston, K. P.; Dai, H. J.; Cochran, H. D.; Melnichenko, Y. B.; Wignall, G. D. *J. Phys. Chem. B* **2001**, *105*, 3540−3548.
(43) da Rocha, S. R. P.; Psathas, P. A.; Klein, E.; Johnston, K. P. *J. Colloid Interface Sci.* **2001**, *239*, 241−253.
(44) da Rocha, S. R. P.; Johnston, K. P.; Westacott, R.; Rossky, P. J. *J. Phys. Chem. B* **2001**, *105*, 12092−12104.
(45) Schurhammer, R.; Berny, F.; Wipff, G. *Phys. Chem. Chem. Phys.* **2001**, *3*, 647−656.
(46) Schurhammer, R.; Wipff, G. *New J. Chem.* **2002**, *26*, 229−233.
(47) Baaden, M.; Schurhammer, R.; Wipff, G. *J. Phys. Chem. B* **2002**, *106*, 434−441.
(48) Salaniwal, S.; Cui, S. T.; Cochran, H. D.; Cummings, P. T. *Langmuir* **2001**, *17*, 1773−1783.
(49) da Rocha, S. R. P.; Johnston, K. P. *Langmuir* **2000**, *16*, 3690−3695.
(50) Berendsen, H. J. C.; Straatsma, T. P. *J. Phys. Chem.* **1987**, *91*, 6269−6271.
(51) Alejandre, J.; Tildesley, D. J.; Chapela, G. A. *J. Chem. Phys.* **1995**, *102*, 4574−4583.
(52) Harris, J.; Young, K. H. *J. Phys. Chem.* **1995**, *99*, 12021−12024.
(53) da Rocha, S. R. P.; Harrison, K. L.; Johnston, K. P. *Langmuir* **1999**, *15*, 419−428.
(54) Deppmeier, B. J. e. a. *SPARTAN*, 5.1.3 ed.; WaveFunction Inc.: Irvine, CA, 1998.
(55) Lee, K.; Sanchez, I. Internal communication.
(56) Koike, A.; Yoneya, M. *J. Chem. Phys.* **1996**, *105*, 6060−6067.
(57) Koike, A. *J. Phys. Chem. B* **1999**, *103*, 4578−4589.
(58) Jorgensen, W.; Gao, J. *J. Phys. Chem.* **1986**, *90*, 2174−2182.
(59) Zielinsky, R. G.; Kline, S. R.; Kaler, E. W.; Rosov, N. *Langmuir* **1997**, *13*, 3934−3937.
(60) Smith, W.; Forester, T. R. *DL_POLY Package for Molecular Dynamics Simulations*, 2.12 ed.; CCLRC, Daresbury Laboratory: Daresbury, Warrington, 1999.
(61) Allen, M. P.; Tildesley, D. J. *Computer Simulation of Liquids*; Clarendon Press: Oxford, 1987.
(62) Chang, T. M.; Dang, L. X. *J. Chem. Phys.* **1996**, *104*, 6772−6783.
(63) Rowlinson, J. S.; Widom, B. *Molecular Theory of Capillarity*; Clarendon Press: Oxford, 1982; Vol. 8.
(64) Croxton, C. A. *Statistical Mechanics of the Liquid Surface*; John Wiley & Sons: Chichester, 1980.
(65) *WebLab ViewPro 4.0*; Molecular Simulations Inc., 2000.
(66) Lu, J. R.; Simister, E. A.; Thomas, R. K.; Penfold, J. *J. Phys.: Condens. Matter* **1994**, *6*, A403−408.
(67) Hou, M. J.; Kim, M.; Shah, D. O. *J. Colloid Interface Sci.* **1988**, *123*, 398−412.
(68) McFann, G. J.; Johnston, K. P.; Howdle, S. M. *AIChE J.* **1994**, *40*, 543−555.
(69) Lu, J. R.; Hromadova, M.; Thomas, R. K.; Penfold, J. *Langmuir* **1993**, *9*, 2417−2425.
(70) Sides, S. W.; Grest, G. S.; Lacasse, M.-D. *Phys. Rev. E* **1999**, *60*, 6708−6713.
(71) Mitrinovic, D. M.; Tikhonov, A. M.; Li, M.; Huang, Z.; Shlossman, M. L. *Phys. Rev. Lett.* **2000**, *85*, 582−584.
(72) Lacasse, M.-D.; Grest, G. S.; Levine, A. J. *Phys. Rev. Lett.* **1998**, *80*, 309−312.
(73) Chittofrati, A.; Lenti, D.; Sanguineti, A.; Visca, M.; Gambi, C. M. C.; Senatra, D.; Zhou, Z. *Prog. Colloid Polym. Sci.* **1989**, *79*, 218−225.
(74) Caporiccio, G.; Burzio, F.; Carniselli; Biancardi, V. *J. Colloid Interface Sci.* **1984**, *98*, 202−209.
(75) Senapati, S.; Berkowitz, M. L. *Phys. Rev. Lett.* **2001**, *87*, 176101-1-4.
(76) Smith, G. D.; Jaffe, R. L.; Yoon, D. Y. *Macromolecules* **1995**, *28*, 5804−5810.
(77) Bandyopadhyay, S.; Shelley, J. C.; Klein, M. L. *J. Phys. Chem. B* **2001**, *105*, 5979−5986.
(78) Kraft, M. P. *Adv. Drug Delivery Rev.* **2001**, *47*, 209−228.
(79) Shin, S.; Collazo, N.; Rice, S. A. *J. Chem. Phys.* **1993**, *98*, 3469−3474.
(80) Smondyrev, A. M.; Berkowitz, M. L. *J. Chem. Phys.* **1999**, *111*, 9864−9870.
(81) O'Neill, M.; Yates., M. Z.; Harrison, K. L.; Johnston, P. K.; Canelas, D. A.; Betts, D. E.; DeSimone, J. M.; Wilkinson, S. P. *Macromolecules* **1997**, *30*, 5050−5059.
(82) Meredith, J. C.; Sanchez, I. C.; Johnston, K. P.; de Pablo, J. J. *J. Chem. Phys.* **1998**, *109*, 6424−6434.
(83) Ulmius, J.; Lindman, B. *J. Phys. Chem.* **1981**, *85*, 4131−4135.
(84) Israelachvili, J. N. *Intermolecular and Surface Forces*, 2nd ed.; Academic Press: San Diego, 1997.
(85) Shelley, J.; Watanabe, K.; Klein, M. L. *Electrochim. Acta* **1991**, *36*, 1729−1734.
(86) Berr, S.; Jones, R. R. M.; Johnson, J. S. J. *J. Phys. Chem.* **1992**, *96*, 5611−5614.